ACS Catalysis

Research Article

pubs.acs.org/acscatalysis

Electrocatalytic Activity and Stability of Titania-Supported Platinum–Palladium Electrocatalysts for Polymer Electrolyte Membrane Fuel Cell

Sheng-Yang Huang, Prabhu Ganesan, and Branko N. Popov*

Center for Electrochemical Engineering, Department of Chemical Engineering, University of South Carolina, Columbia, South Carolina 29208, United States

Supporting Information

ABSTRACT: Titania-supported platinum–palladium electrocatalysts ($PtPd/TiO_2$) were synthesized and investigated as alternative catalysts for the oxygen reduction reaction (ORR). Transmission electron microscope images revealed a uniform distribution of metal nanoparticles (d_M = 3–5 nm) on the TiO_2 support. An increase in ORR activity has been observed with an increase in the Pd content of the bimetallic alloy up to 30%, and beyond this composition, the decrease in catalytic activity has been found to be due to the blocking of Pt active sites by a large amount of Pd in the catalyst. The $PtPd/TiO_2$ electrocatalyst with a Pt/Pd composition of 70:30 shows activity comparable to that of a commercial Pt/C catalyst (TKK) in rotating ring-disk electrode studies. The accelerated durability test results show good stability for the $PtPd/TiO_2$ electrocatalysts at high potentials in terms of minimum loss in the Pt electrochemical surface area. The high stability of the $PtPd/TiO_2$ electrocatalyst synthesized in this investigation offers a new approach to improve the reliability and durability of polymer electrolyte membrane-based fuel cell cathode catalysts.

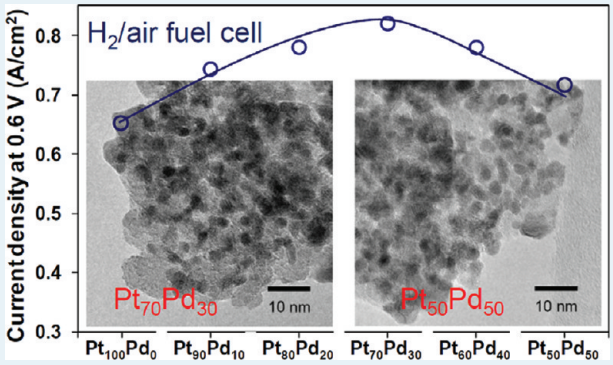

KEYWORDS: *titania, corrosion resistance support, platinum, palladium, oxygen reduction reaction, proton exchange membrane fuel cell*

1. INTRODUCTION

Fuel cells are regarded as clean energy sources for the future. The polymer electrolyte membrane fuel cell (PEMFC) is emerging as a promising candidate in the portable electronics and automobile industries due to its high power density and portability.[1−4] Carbon-supported platinum (Pt/C) and platinum-based alloy catalysts are the most commonly used cathode catalysts for PEMFCs. Alloying Pt with other transition metals, such as Fe, Co, and Ni, can increase the catalytic activity and sometimes the stability of these catalysts for the oxygen reduction reaction (ORR). This effect may be attributed to the formation of alloys with favorable Pt–Pt interatomic distances or Pt crystal orientations in the Pt alloys that facilitate oxygen reduction and mitigate Pt sintering/dissolution.[5−7] Considerable efforts have been made to improve the durability and stability of Pt/C cathode catalysts in PEMFCs. Among all the known reasons for the low electrocatalyst durability, the loss of electrochemical surface area (ECSA) due to corrosion of the catalyst support and subsequent agglomeration of Pt nanoparticles deposited on the support have been recognized as the most important issues to be addressed.[8−10]

Electrochemical oxidation of the carbon support (eq 1)[11−13] causes microstructural degradation and surface chemical changes, which eventually lead to a loss of ECSA.

$$C + 2H_2O \rightarrow CO_2 + 4H^+ + 4e^- \quad (E^0 = 0.207\ \text{V vs NHE at 25 °C}) \tag{1}$$

The corrosion rate of carbon increases drastically at high electrode potentials. Carbon corrosion also leads to electrically isolated Pt particles that are detached from the support. Moreover, it is worth noticing that Pt also plays an important role in accelerating the carbon corrosion.[14,15] These effects result in a rapid degradation of the Pt catalyst and thus shorten the lifetime of the PEMFC.

The cost of Pt-based catalysts is another obstacle for the commercialization of fuel cell vehicles due to the world's limited Pt reserves. Therefore, many recent studies have focused on decreasing Pt loadings and increasing Pt utilization in fuel cells while maintaining satisfactory activity and stability. These efforts include the design of novel catalysts,[16,17] the use of new support materials,[18,19] and the optimization of electrode structure and fabrication methods,[15,20,21] However, it is still

Special Issue: Electrocatalysis

Received: February 5, 2012
Revised: March 22, 2012
Published: April 5, 2012

challenging to obtain a Pt-based fuel cell cathode catalyst with both good durability and high activity.

In this paper, we describe a new approach to address both the activity and stability issues by using titania (TiO_2) as a corrosion-resistant support for Pt−Pd bimetallic catalysts ($PtPd/TiO_2$). These $PtPd/TiO_2$ electrocatalysts displayed substantially enhanced ORR activity as compared with that of a Pt/TiO_2 electrocatalyst. The fuel cell performance of the $PtPd/TiO_2$ catalysts achieves a maximum at a Pt/Pd weight ratio of 70/30.

2. EXPERIMENTAL SECTION

2.1. Synthesis of Titania and Supported Catalyst. Mesoporous TiO_2 was synthesized via a template-assisted route.[22] In the synthesis, the porous structure of TiO_2 was tailored by the controlled hydrolysis of titanium isopropoxide (Alfa Aesar) in the presence of a surfactant (Pluronic P123, BASF). The resulting powder was calcined at 300 °C for 2 h under a nitrogen flow (50 mL/min). We have chosen a new strategy to overcome the low conductivity of TiO_2 (1.47 μS/cm). Metal particles deposited on the TiO_2 surface not only acted as a catalyst for ORR but also provided the path for the electrons. Therefore, electrocatalysts with a metal loading of 60 wt % were prepared in this study. Supported platinum and platinum−palladium electrocatalysts (Pt/TiO_2 and $PtPd/TiO_2$) were prepared by a chemical reduction method using sodium borohydride (Alfa Aesar) as a reducing agent. The details of synthesis procedures for the support and the catalyst are reported elsewhere.[1] The $PtPd/TiO_2$ electrocatalysts with Pt/Pd composition varying from 100:0 to 50:50 and their electrochemical performance as ORR electrocatalysts was studied. The prepared catalysts were named as Pt_xPd_y, in which symbols x and y denote the weight ratio of the Pt and Pd, respectively. For example, $Pt_{100}Pd_0$ represents an electrocatalyst of 60 wt % Pt/TiO_2 while $Pt_{50}Pd_{50}$ indicates an electrocatalysts of 30 wt % Pt and 30 wt % Pd on TiO_2. Table 1 lists the electrocatalysts prepared in this study.

Table 1. Particle Size, ORR Activity, and Open Circuit Voltage (OCV), Fuel Cell Performance of the Various $PtPd/TiO_2$ Electrocatalysts

				current density	
electrocatalysts	particle size (nm)	ORR activity (mA/cm^2)[a]	OCV (V)[a]	at 0.7 V (A/cm^2)[b]	at 0.6 V (A/cm^2)[b]
$Pt_{100}Pd_0$	4.0	2.30	0.925	0.446	0.649
Pt_{90}/Pd_{10}	4.2	2.65	0.924	0.521	0.743
Pt_{80}/Pd_{20}	3.8	3.05	0.926	0.540	0.780
$Pt_{70}Pd_{30}$	3.9	2.95	0.930	0.574	0.820
$Pt_{60}Pd_{40}$	4.2	2.75	0.926	0.510	0.780
$Pt_{50}Pd_{50}$	3.9	2.75	0.925	0.456	0.716

[a]The ORR activity was calculated from the experimental data using the mass-transport correction for rotating disk electrodes. [b]Measurements were taken at 75 °C with fully humidified reactants (flow rate was 150/150 mL/min for H_2/O_2).

2.2. Material Characterization. Physical properties of the TiO_2 and supported catalyst were characterized by BET surface area analysis, X-ray diffraction (XRD), and transmission electron microscopy (TEM). BET surface area measurements were performed using a Quantachrome NOVA 2000 BET analyzer. XRD analysis was performed using a Rigaku X-ray diffractometer at 2θ ranging between 20° and 80° using Cu K_α radiation. A tube voltage of 30 kV and a current of 15 mA were used during the scanning. TEM was carried out using a JEOL-2100F microscope equipped with a field emission electron gun source and operated at 200 kV. The metal loading of electrocatalysts was determined by inductively coupled plasma atomic emission spectrometry (ICP-AES).

2.3. Electrochemical Characterization. The electrochemical properties of the electrocatalysts were characterized by cyclic voltammetry (CV) and linear sweep voltammetry (LSV) techniques. All the electrochemical characterization studies were performed in 0.5 M H_2SO_4 using a Pine bipotentiostat (model AFCBP1), a Pt-wire counter electrode, and a Hg/Hg_2SO_4 reference electrode [0.68 V vs reversible hydrogen electrode (RHE)]. A rotating ring-disk electrode (RRDE) with a Pt ring and a glassy carbon disk (0.247 cm^2) was used as the working electrode. The catalyst ink was prepared by blending the catalyst powder [Pt/TiO_2, $PtPd/TiO_2$, or Pt/C (50 wt % Pt/C, TEC10E50E, TKK)] with ethanol in an ultrasonic bath. Cyclic voltammograms recorded in nitrogen were used to obtain the background capacitive currents and ECSA of the Pt catalysts.

The ECSA of Pt was determined by charge integration under the hydrogen desorption peaks appearing between 0.05 and 0.35 V by assuming a charge of 210 $\mu C/cm^2$ for the electroactive Pt surface. Then the specific ECSA was calculated on the basis of the following relation:

$$\text{specific ECSA} = \frac{Q_H}{m \times q_H} \quad (2)$$

where Q_H is the charge for hydrogen desorption, m is the Pt metal loading, and q_H is the charge required for desorbing a monolayer of hydrogen on the Pt surface. The electrolyte was purged with oxygen for 30 min prior to the oxygen reduction measurement. The oxygen reduction current was calculated from the difference between currents measured in the nitrogen- and oxygen-saturated electrolytes. All the potential values mentioned in the RRDE study are referred to an RHE.

2.4. PEM Fuel Cell Operation. A commercially available gas diffusion layer (GDL; Sigracet GDL 10BC, SGL) was used for the fuel cell experiments. The anode catalyst loading was 0.4 mg_{Pt}/cm^2 (50 wt % Pt/C, TKK). The cathode catalyst ink was prepared by ultrasonically blending 0.15 g of electrocatalyst powder with a Nafion solution (5 wt %, Alfa Aesar) and ethanol for 4 h. The catalyst ink was then sprayed onto a GDL. The process was repeated until the desired metal loading was achieved (0.4 mg/cm^2). The anode and cathode electrodes were hot-pressed onto both sides of a Nafion 212 membrane at 140 °C under 200 psi for 3 min. The MEA was then cooled to room temperature and assembled in 5 cm^2 single cells for performance evaluation and stability studies, respectively. H_2 (150 mL/min) and air (300 mL/min) humidified at 75 °C were supplied to the anode and cathode compartments, respectively. Polarization experiments were conducted using a fully automated test station (Fuel Cell Technologies Inc.) at 75 °C.

2.5. Stability and Durability Tests for Catalysts. The electrochemical stability and performance of the $Pt_{100}Pd_0$, $Pt_{70}Pd_{30}$, and commercial Pt/C cathode catalysts were examined using an in-house-developed accelerated durability test (ADT) by continuously cycling the potential between 0.6 and 1.4 V with periodic measurements of ECSA and catalytic

dx.doi.org/10.1021/cs300088n | ACS Catal. 2012, 2, 825−831

activity in half-cell testing conditions. Under these conditions, the deterioration of the catalysts was accelerated. Under half-cell conditions (in RRDE), the potential cycling was carried out for 1500 cycles in 0.5 M H_2SO_4 at a scan rate of 50 mV/s. Nitrogen gas was bubbled into the electrolyte throughout the experiment.

3. RESULTS AND DISCUSSION

3.1. Characterization of TiO_2 and Pt/TiO_2. The bright-field TEM micrographs of TiO_2, $Pt_{100}Pt_0$, $Pt_{70}Pd_{30}$, and $Pt_{50}Pd_{50}$ are shown in Figure 1. Aggregation of granular TiO_2 was

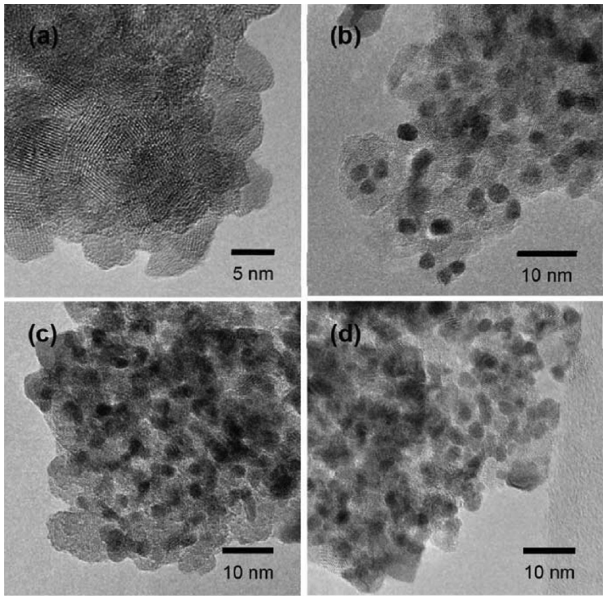

Figure 1. Transmission electron micrographs of (a) TiO_2, (b) $Pt_{100}Pd_0$, (c) $Pt_{70}Pd_{30}$, and (d) $Pt_{50}Pd_{50}$ electrocatalysts.

observed in the TEM image. The particle size of the synthesized TiO_2 particles was in the range between 7 and 15 nm with a BET surface area of 186 m^2/g. The TEM images shown in Figure 1b–d revealed the successful deposition of Pt and Pt–Pd particles onto the TiO_2 support. Metal nanoparticles were uniformly distributed on the TiO_2 surface. In addition, the metal particles are in the range of 3–5 nm, regardless of the Pt/Pd weight ratios. It is well-known that the mass activity of Pt catalysts for ORR shows a maximum at a Pt particle size of 3–4 nm.[23] Therefore, the Pt/TiO_2 and PtPd/TiO_2 were expected to show a good ORR activity.

Figure 2 compares the XRD patterns of the TiO_2 and various PtPd/TiO_2 electrocatalysts. The XRD pattern of TiO_2 indicates the presence of an anatase phase, as confirmed by the observation of the most intense peak of anatase (101) 2θ = 25.3°. The influence of the metal compositions on the crystalline phase and particle size of the PtPd was investigated using XRD. XRD pattern shows diffraction peaks of face-centered cubic (fcc) lattice for the various PtPd/TiO_2 electrocatalysts. The average particle of metal (d_M, 4.0 nm for $Pt_{100}Pd_0$) was calculated from the peak width of Pt (220) using Debye–Scherrer equation.[24] The d_M was calculated to be 3.9 nm for both $Pt_{70}Pd_{30}$ and $Pt_{50}Pd_{50}$. Table 1 summarizes the metal particle sizes obtained from XRD. It can be seen from the Table that the PtPd/TiO_2 electrocatalysts exhibit particle sizes comparable to that of Pt/TiO_2. This confirms that the TiO_2 is a suitable support for preparing high-dispersion Pt or Pt-based

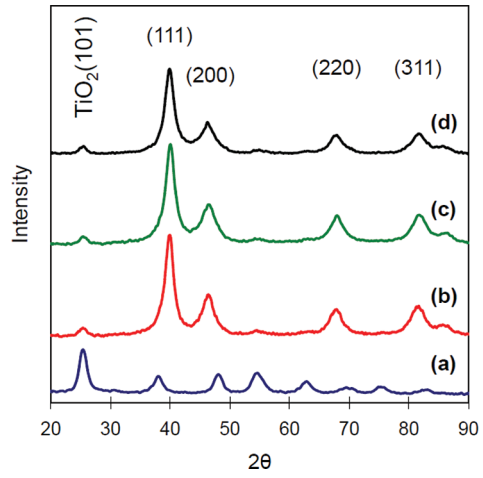

Figure 2. X-ray diffraction patterns of (a) TiO_2, (b) $Pt_{100}Pd_0$, (c) $Pt_{70}Pd_{30}$, and (d) $Pt_{50}Pd_{50}$ electrocatalysts.

catalysts with smaller particle sizes. The effect of metal composition on peak position is insignificant because both metals have an fcc phase with a unit length of 3.92 Å for Pt and 3.89 Å for Pd.

3.2. Electrochemical Studies. Figure 3a shows the ORR polarization curves for the various PtPd/TiO_2 electrocatalysts. The ORR curves were under mixed kinetic diffusion control reaction in the potential region between 0.95 and 0.60 V, followed by a region in which the diffusion-limiting current (~3.7 mA/cm^2) was observed. The increase in ORR activity has been observed with increase in Pd content of the bimetallic alloy up to 30%, and beyond this composition, a decrease in catalytic activity has been found (Table 1). Figure 3b compares the ORR activities in the region between 0.75 and 0.95 V. The activities were calculated from the experimental data using the mass-transport correction for rotating disk electrodes using the following equations:[25]

$$\frac{1}{i} = \frac{1}{i_k} + \frac{1}{i_d} \tag{3}$$

$$i_k = \frac{i_d i}{i_d - i} \tag{4}$$

where i is the measured current during the ORR, i_k is the mass-transport free kinetic current, and i_d is the diffusion-limited current. Activities (A) can be determined by calculating the i_k using eq 4. As can be seen in Figure 3b, the activity of the various PtPd/TiO_2 at 0.85 V (2.65–3.05 mA/cm^2) was higher than that of the Pt/TiO_2 (2.30 mA/cm^2).

Figure 4 shows the polarization and power density plots of the PEM fuel cells employing PtPd/TiO_2 cathode electrocatalysts. The $Pt_{100}Pd_0$ electrocatalyst generated 0.65 A/cm^2 at 0.60 V and a maximum power density of 0.39 W/cm^2 when fuel cell was feed with hydrogen and air. The maximum power density of the $Pt_{70}Pd_{30}$ was 0.52 W/cm^2, which is ~133% that generated when employing $Pt_{100}Pd_0$ as the cathode catalysts. The polarization curves demonstrated good ORR kinetics and fuel cell performance for the PtPd/TiO_2 electrocatalysts synthesized in this study. The fuel cell results also indicated that deposited metal particles provided an adequate electron pathway and improved the electrical conductivity of the TiO_2 support.

dx.doi.org/10.1021/cs300088n | ACS Catal. 2012, 2, 825–831

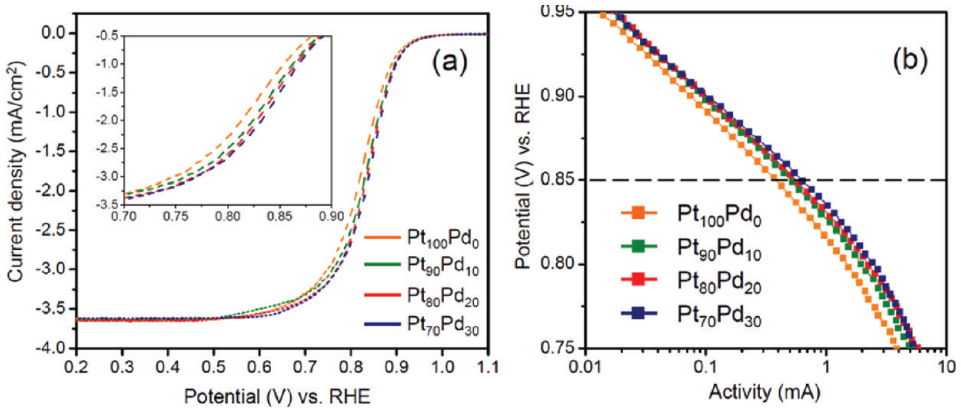

Figure 3. (a) ORR polarization curves for the various PtPd/TiO_2 electrocatalysts recorded at room temperature in an O_2-saturated 0.5 M H_2SO_4 solution with a sweep rate of 5 mV/s and a rotation rate of 900 rpm. The Pt loading on each RRDE was 100 $\mu g/cm^2$. Part a in the upper-left corner shows polarization curves between 0.7 and 0.9 V. (b) Activities of ORR measurements shown for the various PtPd/TiO_2 electrocatalysts obtained from part a.

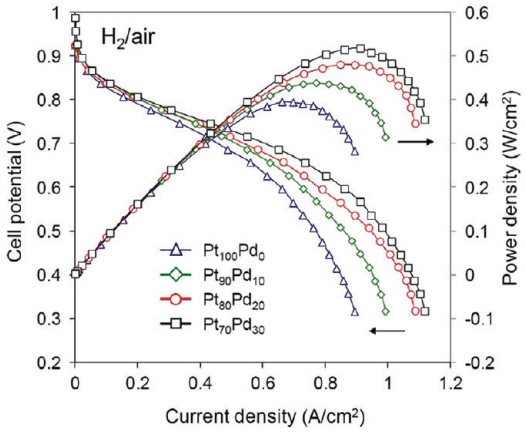

Figure 4. Polarization and power density curves of the PEM fuel cells with the various PtPd/TiO_2 cathode electrocatalysts. Measurements were taken at 75 °C with fully humidified reactants (flow rate was 150/300 mL/min for H_2/air). Catalyst loading was controlled at 0.4 mg/cm^2 on both the electrodes. No backpressure was applied during fuel cell operation.

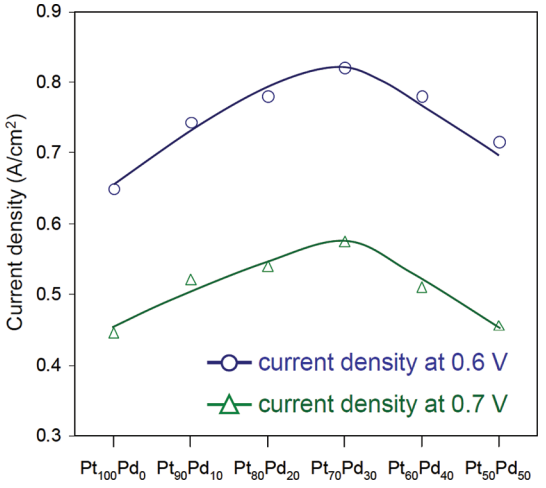

Figure 5. Effect of Pt/Pd weight ratio on the PEM fuel-cell performance with the various PtPd/TiO_2 cathode electrocatalysts.

For comparison, the current densities of the PtPd/TiO_2 cathodes at cell voltages of 0.6 and 0.7 V are plotted as a function of the Pt/Pd weight ratio (Figure 5). It is clearly seen here that the cell performance increased with the increase in Pd content in the metal composition and reached a maximum activity at 30 wt %; further increases in the Pd content resulted in a decrease of the fuel cell performance. ORR on palladium metal has been studied, and yet, Pd shows rather poor catalytic activity in comparison with Pt metals.[26,27] Therefore, it seems reasonable to hypothesize that the variation in ORR activity might be caused by the blocking of Pt active sites by a large amount of Pd in the catalyst. Crooks et al.[26] reported that improvements in ORR activity have been associated with Pt-based alloys. Some interpretations of these effects include shifts of core levels due to a charge transfer between Pt and second metal[28] or changes in the density of states near the Fermi level.[29] An increased 5d vacancy of Pt, as a result of its interaction with a second metal, is believed to increase the interaction of O_2 and Pt, thereby enhancing the catalytic activity of a Pt "skin" on a PtPd alloy.[27] The improved ORR kinetics of the PtPd compared with Pt could be due to changes in the bond lengths and have also been suggested in the literature.[27,30,31]

Figure 6 shows the polarization and power density plots for H_2−O_2 fuel cells, employing $Pt_{100}Pd_0$, $Pt_{70}Pd_{30}$, and Pt/C (TKK) as the cathode electrocatalyst. The measurements were taken at 75 °C with fully humidified reactants (flow rate was 150/150 mL/min for H_2/O_2). Detailed fuel cell performance measured for $Pt_{100}Pd_0$, $Pt_{70}Pd_{30}$, and Pt/C electrocatalysts are tabulated in Supporting Information Table S1. The observed maximum power density varied with the cathode electrocatalysts and demonstrated the following trend:

$$\begin{aligned} &Pt_{70}Pd_{30}(1.15\ W/cm^2) \\ &> Pt/C(1.10\ W/cm^2) \\ &> Pt_{100}Pd_0(1.03\ W/cm^2) \end{aligned} \quad (5)$$

Although the particle size of the $Pt_{100}Pd_0$ and $Pt_{70}Pd_{30}$ electrocatalysts was large ($d_{PtPd} \approx 4$ nm), they showed fuel cell performance comparable to that of the commercial Pt/C (TKK) electrocatalyst ($d_{Pt} = 2.5$ nm). In the case of Pt/C, the catalyst layer thickness was ~11 μm at a desired Pt loading of 0.4 mg/cm^2, whereas an ultrathin catalyst layer (~1 μm) could be prepared for the TiO_2-supported electrocatalysts at the same

dx.doi.org/10.1021/cs300088n | ACS Catal. 2012, 2, 825−831

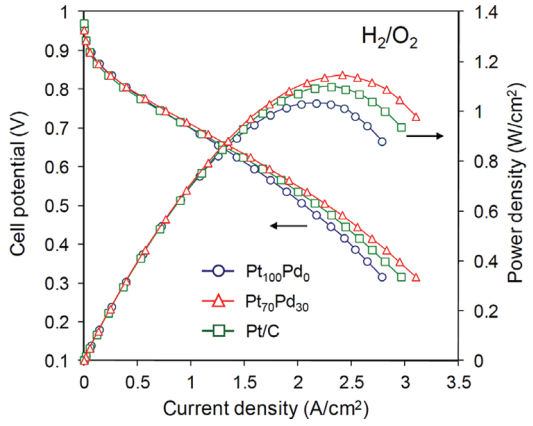

Figure 6. Polarization and power density curves of the PEM fuel cells using $Pt_{100}Pt_0$, $Pt_{70}Pd_{30}$, and Pt/C cathode electrocatalysts. Measurements were taken at 75 °C with fully humidified reactants (flow rate was 150/150 mL/min for H_2/O_2). Catalyst loading was controlled at 0.4 mg/cm^2 on the anode side and 0.4 mg/cm^2 on the cathode side. No backpressure was applied during fuel cell operation.

Pt loading, since TiO_2 has a 2-fold higher density than carbon.[32] Debe et al.[33] have reported that fuel-cell performance is strongly affected by the catalyst-layer thickness. In their study, an ultrathin cathode-catalyst layer (~0.27 μm) consisting of nonconductive polymer-supported Pt catalysts (Pt/NP, d_{Pt} = 8 nm) allowed 100% catalyst utilization with a reduction in the mass transport overpotential losses at high current densities. Similarly, the high fuel cell performance of the $Pt_{100}Pd_0$ and $Pt_{70}Pd_{30}$ electrocatalysts can be attributed to the low mass transport limitation in the cathode at high current density (>0.6 A/cm^2). Furthermore, the fuel cell results suggested that $Pt_{70}Pd_{30}$ electrocatalyst displayed substantially enhanced performance as compared with that of $Pt_{100}Pd_0$ electrocatalyst.

3.3. Comparison of Catalyst Stability Using Accelerated Durability Test. Figure 7 shows the subset of CVs for the $Pt_{100}Pt_0$, $Pt_{70}Pd_{30}$, and Pt/C electrocatalysts obtained at room temperature during continuous cycling between 0.6 and 1.4 V for a total of 1500 cycles. The CV curves of $PtPd/TiO_2$ in Figure 7a and b showed the usual voltammograms for Pt in acid electrolytes, and no additional current peak was observed. All electrocatalysts exhibited a reduction in the hydrogen underpotential deposition area with repeated potential cycling. The ECSAs of $Pt_{100}Pd_0$, $Pt_{70}Pd_{30}$, and Pt/C after potential cycling experiments were calculated from the hydrogen desorption peaks.

The ECSAs are plotted as a function of cycle number in Figure 8a. As can be seen from the figure, all the catalysts exhibited a decrease in ECSA with increased cycle number. During the CV measurements, these catalysts were exposed to extremely corrosive conditions. By polarizing the catalyst in acidic media, the corrosion of the carbon support resulted in decreased catalyst active surface area due to catalyst particle sintering. A variety of mechanisms for Pt dissolution and redeposition on the catalyst surface and Pt migration through the surface have been suggested[34] to explain the increase in the catalyst particle size over exposure time. One such mechanism is the Pt dissolution into the electrolyte from the supported Pt catalysts and then redeposition on the surface of larger particles, a phenomenon known as Ostwald ripening.[17] After 1500 cycles, a huge loss in the ECSA (~95%) was observed for the Pt/C catalyst, confirming the corrosion of high-surface-area carbon

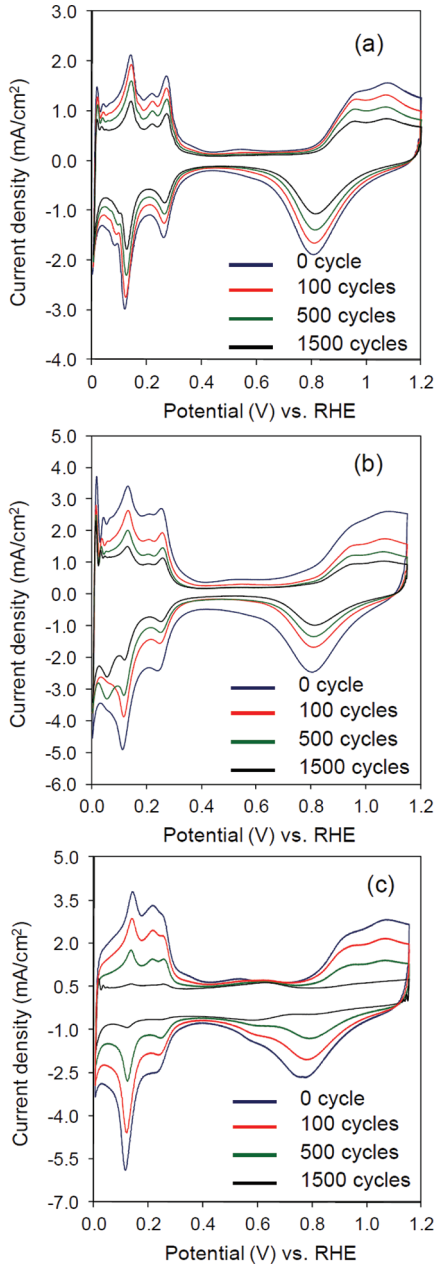

Figure 7. Series of CV plots obtained at room temperature after 0.6–1.4 V cycling at 50 mV/s under N_2: (a) $Pt_{100}Pd_0$, (b) $Pt_{70}Pd_{30}$, and (c) Pt/C. Cyclic voltammetry was conducted in the potential range between 0.0 and 1.2 V at a scan rate of 50 mV/s.

support at high positive potentials (>1.0 V) and subsequent processes, such as Ostwald ripening, Pt particle migration, and sintering (Figure 8a). In contrast, comparatively smaller loss in ECSA observed for the $Pt_{100}Pt_0$ and $Pt_{70}Pd_{30}$ indicated their higher electrochemical stability than the Pt/C.

Periodic measurement of ORR activity was performed initially and after every 500 cycles during the ADT. Figure 8b compares the ORR activities at 0.85 V. The activities were calculated from the experimental data using the mass-transport correction for rotating disk electrodes using eq 4. ECSA and ORR current density of the $Pt_{100}Pd_0$, $Pt_{70}Pd_{30}$, and Pt/C electrocatalysts measured during potential cycling experiments are summarized in Table 2. As can be seen in Figure 8b, the activity of the $Pt_{70}Pd_{30}$ at 0.85 V (3.05 mA/cm^2) was

dx.doi.org/10.1021/cs300088n | ACS Catal. 2012, 2, 825–831

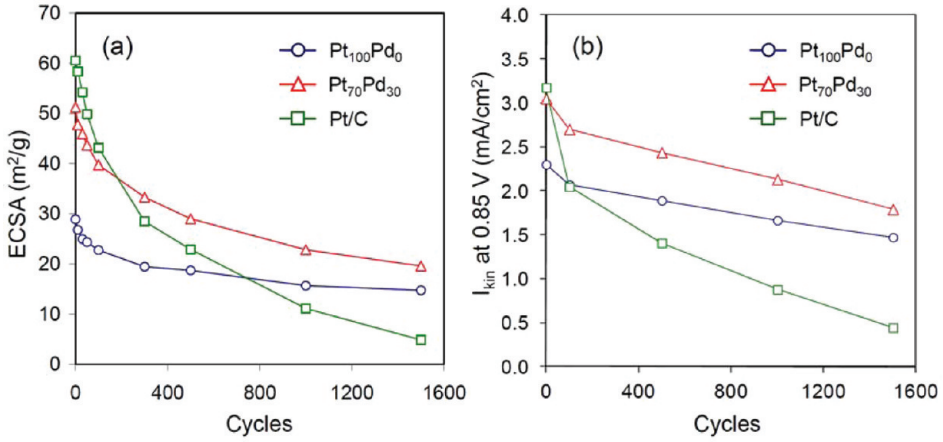

Figure 8. (a) Pt electrochemical surface area and (b) current density at 0.85 V as a function of the number of CV cycles for PtPd/TiO_2 and Pt/C electrocatalysts measured during potential cycling experiments.

Table 2. ECSA and ORR Current Density (at 0.85 V) of the $Pt_{100}Pd_0$, $Pt_{70}Pd_{30}$, and Pt/C Electrocatalysts Measured During Potential Cycling Experiments

	ECSA (m^2/g)			current density (mA/cm^2)		
cycle numbers	$Pt_{100}Pd_0$	$Pt_{70}Pd_{30}$	Pt/C	$Pt_{100}Pd_0$	$Pt_{70}Pd_{30}$	Pt/C
0	28.9	51.2	60.6	2.30	3.05	3.18
100	22.8	39.7	43.1	2.07	2.70	2.05
500	18.7	29.0	22.9	1.89	2.44	1.41
1000	15.7	22.8	11.1	1.67	2.13	0.88
1500	14.7	19.6	4.9	1.47	1.79	0.44

comparable to that of the Pt/C (3.18 mA/cm^2). To estimate the effect of the ADT on the oxygen reduction activity, the loss of ORR activity at 0.85 V was calculated using the following equation:

$$\mathrm{ORR_{loss}}\% = 100 - \frac{A_x}{A_0} \times 100 \quad (6)$$

where A_0 and A_x are the initial activity and the activity after x cycles, respectively. At the beginning of the ADT, the activity decreased rapidly for the first 500 cycles until it reached a slow but steady decay. The ORR activity of PtPd/TiO_2 was found to be 1.79 mA/cm^2 after 1500 cycles, whereas the Pt/C showed a loss of ~86% of its initial activity (from 3.18 to 0.44 mA/cm^2) due to carbon corrosion and subsequent catalyst particle sintering and agglomeration. In addition, the PtPd/TiO_2 showed 4-fold higher ORR activity than the Pt/C catalyst after the potential cycling experiment.

4. CONCLUSION

In this study, electrocatalysts with various Pt/Pd compositions were synthesized and investigated as cathode catalysts for PEMFCs. The TEM images of the PtPd/TiO_2 electrocatalysts revealed a uniform distribution of metal particles (d_M = 3–5 nm) onto the TiO_2 support. The increase in ORR activity has been observed with an increase in the Pd content of the bimetallic alloy up to 30%, and beyond this composition, the decrease in catalytic activity has been found due to the blocking of Pt active sites by a large amount of Pd in the catalyst. Furthermore, the $Pt_{70}Pd_{30}$ catalyst showed activity similar to that of a conventional Pt/C catalyst (TKK) in half-cell studies. The ADT experiment conducted in an RRDE demonstrated high stability and catalytic activity for the Pt/TiO_2 and PtPd/TiO_2 electrocatalysts. The $Pt_{70}Pd_{30}$ showed a 4-fold higher ORR activity than the Pt/C after subjecting both catalysts to a potential cycling experiment. The ADT and fuel cell performance results of the PtPd/TiO_2 electrocatalyst demonstrated an improvement in durability and stability for PEM-based fuel cell cathode catalysts.

■ ASSOCIATED CONTENT

Supporting Information

ORR activity plots and fuel cell performance. This material is available free of charge via the Internet at http://pubs.acs.org.

■ AUTHOR INFORMATION

Corresponding Author

*Phone: +1 803 777 7314. Fax: +1 803 777 8265. E-mail: popov@cec.sc.edu.

Notes

The authors declare no competing financial interest.

■ ACKNOWLEDGMENTS

Financial support from National Science Foundation (CBET, 0966956) and NASA-EPSCoR (NNX07AT68A) is gratefully acknowledged.

■ REFERENCES

(1) Huang, S. Y.; Ganesan, P.; Park, S.; Popov, B. N. *J. Am. Chem. Soc.* **2009**, *131*, 13898–13899.
(2) Lubitz, W.; Tumas, W. *Chem. Rev.* **2007**, *107*, 3900–3903.
(3) Gasteiger, H. A.; Kocha, S. S.; Sompalli, B.; Wagner, F. T. *Appl. Catal., B* **2005**, *56*, 9–35.
(4) Huang, S. Y.; Chang, S. M.; Lin, C. L.; Chen, C. H.; Yeh, C. T. *J. Phys. Chem. B* **2006**, *110*, 23300–23305.
(5) Jalan, V.; Taylor, E. J. *J. Electrochem. Soc.* **1983**, *130*, 2299–2301.
(6) Beard, B. C.; Ross, P. N. *J. Electrochem. Soc.* **1990**, *137*, 3368–3374.
(7) Toda, T.; Igarashi, H.; Uchida, H.; Watanabe, M. *J. Electrochem. Soc.* **1999**, *146*, 3750–3756.
(8) Chalk, S. G.; Miller, J. E. *J. Power Sources* **2006**, *159*, 73–80.
(9) Wilson, M. S.; Garzon, F. H.; Sickafus, K. E.; Gottesfeld, S. *J. Electrochem. Soc.* **1993**, *140*, 2872–2877.
(10) Siroma, Z.; Ishii, K.; Yasuda, K.; Miyazaki, Y.; Inaba, M.; Tasaka, A. *Electrochem. Commun.* **2005**, *7*, 1153–1156.
(11) Kinoshita, K. *Carbon: Electrochemical and Physicochemical Properties*. John Wiley & Sons: New York: 1988.
(12) Kinoshit., K; Bett, J. A. S. *Carbon* **1973**, *11*, 403–411.

(13) Pyun, S. I.; Lee, E. J.; Kim, T. Y.; Lee, S. J.; Ryu, Y. G.; Kim, C. S. *Carbon* **1994**, *32*, 155−159.
(14) Ferreira, P. J.; la O, G. J.; Shao-Horn, Y.; Morgan, D.; Makharia, R.; Kocha, S.; Gasteiger, H. A. *J. Electrochem. Soc.* **2005**, *152*, A2256−A2271.
(15) Shao, Y. Y.; Yin, G. P.; Gao, Y. Z. *J. Power Sources* **2007**, *171*, 558−566.
(16) Shao, M.; Sasaki, K.; Marinkovic, N. S.; Zhang, L.; Adzic, R. R. *Electrochem. Commun.* **2007**, *9*, 2848−2853.
(17) Chen, Z. W.; Waje, M.; Li, W. Z.; Yan, Y. S. *Angew. Chem., Int. Ed.* **2007**, *46*, 4060−4063.
(18) Huang, S. Y.; Ganesan, P.; Popov, B. N. *Appl. Catal., B* **2009**, *93*, 75−81.
(19) Huang, S. Y.; Ganesan, P.; Popov, B. N. *Appl. Catal., B* **2010**, *96*, 224−231.
(20) Yu, X. W.; Ye, S. Y. *J. Power Sources* **2007**, *172*, 145−154.
(21) Wee, J. H.; Lee, K. Y.; Kim, S. H. *J. Power Sources* **2007**, *165*, 667−677.
(22) Jang, J.; Bae, J. *Chem. Commun.* **2005**, 1200−1202.
(23) Mayrhofer, K. J. J.; Blizanac, B. B.; Arenz, M.; Stamenkovic, V. R.; Ross, P. N.; Markovic, N. M. *J. Phys. Chem. B* **2005**, *109*, 14433−14440.
(24) Huang, S. Y.; Chang, C. M.; Wang, K. W.; Yeh, C. T. *ChemPhysChem* **2007**, *8*, 1774−1777.
(25) Gojkovic, S. L.; Zecevic, S. K.; Savinell, R. F. *J. Electrochem. Soc.* **1998**, *145*, 3713−3720.
(26) Ye, H. C.; Crooks, R. M. *J. Am. Chem. Soc.* **2007**, *129*, 3627−3633.
(27) Zhang, J.; Mo, Y.; Vukmirovic, M. B.; Klie, R.; Sasaki, K.; Adzic, R. R. *J. Phys. Chem. B* **2004**, *108*, 10955−10964.
(28) Rodriguez, J. A. *Surf. Sci. Rep.* **1996**, *24*, 225−287.
(29) Ruckman, M. W.; Strongin, M. *Acc. Chem. Res.* **1994**, *27*, 250−256.
(30) Zhang, J. L.; Vukmirovic, M. B.; Xu, Y.; Mavrikakis, M.; Adzic, R. R. *Angew. Chem., Int. Ed.* **2005**, *44*, 2132−2135.
(31) Zhang, J. L.; Vukmirovic, M. B.; Sasaki, K.; Nilekar, A. U.; Mavrikakis, M.; Adzic, R. R. *J. Am. Chem. Soc.* **2005**, *127*, 12480−12481.
(32) Huang, S. Y.; Ganesan, P.; Popov, B. N. *Appl. Catal., B* **2011**, *102*, 71−77.
(33) Debe, M. K.; Schmoeckel, A. K.; Vernstrorn, G. D.; Atanasoski, R. *J. Power Sources* **2006**, *161*, 1002−1011.
(34) Colon-Mercado, H. R.; Popov, B. N. *J. Power Sources* **2006**, *155*, 253−263.